Inverse Design of Broadband Dispersion Compensation Fiber Based on Deep Learning and Differential Evolution Algorithm

Fuxiao Ma, Yunjie Ma, Peili Li, and Weihua Shi

***Abstract*—A Ge-doped dual-core dispersion compensation photonic crystal fiber (DC-DCPCF) is proposed. The small diameters of two layers' air holes make DC-DCPCF form a dual-core structure, which is conducive to broadband dispersion compensation. Low Ge-doped silica as the only background material reduces the preparation difficulty and cost. It is inversely designed by using artificial neural network (ANN) combined with differential evolution algorithm (DE) to obtain target dispersion compensation. ANN replaces the finite element method to accomplish fast forward prediction of DC-DCPCF properties. DE solves the single solution problem of single or cascade network that makes it flexible and reproducible. The results demonstrate that the designed DC-DCPCF can not only compensate 45 and 25 times its length of Corning single-mode fiber 28 (SMF28) in S+C+L+U bands and E+S+C+L+U bands respectively, but also accurately compensate the residual dispersion with effective dispersion compensation being only +0.005∼+0.842ps/(nm·km) and −0.03∼+1.31ps/(nm·km), respectively. In addition, the kappa values of DCP-PCF are well matched with SMF28 in the broadband wavelength range. It takes only about 10 seconds to complete the inverse design of the target DC-DCPCF. It provides a design method for custom DC-DCPCF and an efficient inverse design solution for photonic automation in fiber optical communication systems.**

***Index Terms*—Deep learning, differential evolution algorithm, dual-core dispersion compensation fiber, enter keywords or phrases in alphabetical order, inverse design, photonic crystal fiber.**

I. Introduction

IN MODERN optical fiber communication systems, especially in long-range transmission systems such as dense wavelength division multiplexing (DWDM), dispersion compensation is of crucial importance [1], [2], [3]. Since the conventional single mode fiber has dispersion accumulation at each wavelength in the optical fiber transmission link, it is necessary to compensate not only the dispersion but also the dispersion slope [4], [5]. In consequence, some designs of dual-core dispersion compensation photonic crystal fiber (DC-DCPCF). By adjusting the refractive index between the inner and outer cores filled with different materials or by changing the diameter of air holes in a certain layer to form dual-core structure, the dual-core PCF can better solve the problem of dispersion compensation over the broad wavebands. Wang et al. proposed an all-solid dual concentric core DCPCF [6] which can compensate 15.43 times its length of SMF28 with small residual dispersion in the range of ±0.15 ps/(nm·km) over S+C bands. However, it is difficult to fabricate because of this structure with a Ge-doped fiber core and a F-doped cladding. A sandwiched photonic crystal fiber [7] was designed for broadband dispersion compensation over S+C+L+U bands, which exhibits an effective compensated dispersion of −0.5∼+0.1 ps/(nm·km) and the dispersion compensation multiple of 25.37. In Reference [8], a PCF with Ge-doped concentric ring outer core shows an effective compensated dispersion range of ±1.38 ps/(nm·km) over S+C+L bands. Habib et al. [9] proposed a hybrid octagonal DC-DCPCF with a square fiber core, which shows an effective compensated dispersion ranges from −1.5 to +0.1 ps/(nm·km) over the E+S+C+L+U bands and its dispersion compensation multiple is 16.92. Even though the above references maintain low effective compensated dispersion, it is essential to improve the band width as well as the dispersion compensation multiple.

In the research of DC-DCPCF, the traditional control variable method is mainly used to optimize its different parameters one by one. It requires a large number of repeated numerical simulations, and is essentially a large number of trial-and-error and time-consuming process. Not only does it rely on the researcher's experience to a high degree, but also it is difficult to obtain the excellent performance of the multi-parameter DC-DCPCF. So inversely designing multiple parameters by optimization algorithms is proposed to obtain a DC-DCPCF with highly similar performance to the target dispersion compensation by finite iterations of the FEM [10]. Although the search efficiency and accuracy of the optimal solution are improved, with the increase of DC-DCPCF structure parameters, the long-time numerical simulation and FEM still occupy a large number of computational resources, and the efficiency of the optimal search needs to be further improved.

In recent years, with the rapid development of artificial intelligence, artificial neural network (ANN) has been widely used in the fields of metasurface [11], nanophotonics [12], and optical communication networks [13], [14]. ANN also has a

Manuscript received 27 February 2023; revised 10 May 2023; accepted 13 May 2023. Date of publication 25 May 2023; date of current version 2 June 2023. This work was supported in part by the Postgraduate Research and Practice Innovation Program of Jiangsu Province under Grants KYCX22_0989, KYCX22_0909, and SJCX21_0277. *(Corresponding author: Peili Li.)*

The authors are with the College of Electronic and Optical Engineering and College of Flexible Electronics (Future Technology), Nanjing University of Posts and Telecommunications, Nanjing 210023, China (e-mail: 2021020301@njupt.edu.cn; 1220024417@njupt.edu.cn; lipl@njupt.edu.cn; shiwh@njupt.edu.cn).

Digital Object Identifier 10.1109/JPHOT.2023.3277129

great advantage in the inverse design of structurally complex, multi-target, and multi-parameter optical fibers. Single ANN [15], [16] has the issue of non-unique solutions with different PCF structures corresponding to the same performance in the inverse mapping process, which can lead to difficulties in convergence of the ANN model. Therefore, cascade network using a pre-trained forward prediction network with an inverse design network [17], [18] can effectively overcome problems such as poor model convergence. However, it can only output a set of fixed structures corresponding to the target performance, and cannot analyze different PCF structures with the same performance. Meanwhile, for the optical response of different targets, the network model needs to be trained using the rebuilt corresponding data sets which is lack of certain universality.

Moreover, ANN can be applied not only for inverse design of PCF, but also for forward prediction which establishes a fast mapping between the design parameters and the properties of PCF [19], [20]. The complicated numerical simulation of FEM can be substituted by ANN to further enhances the computational rate. With the combination of ANN and optimization algorithms [21], the problem of single-solution in single or cascade network is solved. Meanwhile, multiple optimization objectives of DC-DCPCF can be taken into account, and the single ANN which is used for forward prediction can be put into use by training only once. So, the ANN with optimization algorithm can obtain multiple solutions and has better network adaptability.

In this paper, a Ge-doped dual-core dispersion compensation photonic crystal fiber(DC-DCPCF) is proposed. By removing the innermost air hole to form a solid core structure, and reducing the diameters of the second- and third-layer' air holes to form a dual-core structure, DC-DCPCF is high suitable for compensating the dispersion of SMF28 over the broad wavebands. Low Ge-doped silica is used as background material, which can effectively reduce the preparation difficulty and production cost. And the inverse design method with ANN forward prediction combining DE is used to inversely design DC-DCPCF. The use of ANN replacing FEM enables fast forward prediction of the effective refractive index, dispersion and confinement loss of the fundamental mode, resulting in time savings for repeated simulations. Using DE algorithm, the design parameters of DC-DCPCF are inversely designed to obtain DC-DCPCF for different wavebands which has a high match with the target dispersion and confinement loss. The combination of ANN and DE enables fast inverse search for specific targets with a certain degree of repeatability.

II. Principle and Method

A. Design of DC-DCPCF

Fig. 1(a) shows the cross-section of the proposed hexagonal DC-DCPCF. Ge-doped silica is used as the background material of DC-DCPCF. The cladding is a periodic triangular structure which is composed of five layers of air holes. A solid core is formed by removing the innermost air hole. Define Λ as the distance between two adjacent air holes, d_2, and d_3 as the diameters of second- and third-layer air hole, respectively. In order to reduce the difficulty of fabrication, the air hole's diameters in

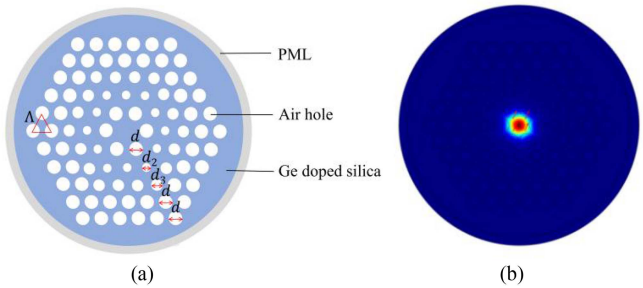

Fig. 1. (a) Cross-section of the DC-DCPCF with germanium doping. (b) Electric field distribution of fundamental mode.

the rest layers are set to the same size with $d_1 = d_4 = d_5 = d$ and are reduced ($d > d_2$, d_3) to form the dual-core structure PCF which contribute to obtaining large negative dispersion for dispersion compensation in broad wavebands.

Define X (mol%) as the mole fraction of GeO_2, and the background material's refractive index can be defined by Sellmeier equation [22]:

$$n^2 = \sum_{i=1}^{3} \frac{SA_i + X * (GA_i - SA_i)\,\lambda^2}{\lambda^2 - (SL_i + X * (GL_i - SL_i))} + 1. \quad (1)$$

where SA_i, SL_i, GA_i and GL_i are coefficients of SiO_2 and GeO_2, λ is wavelength. The Ge-doped DC-DCPCF can been successfully fabricated by modified chemical vapor deposition [23]. Compared to the multi-material PCF with Ge-doped core and pure silica cladding [24], the proposed DC-DCPCF, which consists of the single Ge-doped silica as cladding, has lower fabrication difficulty and production cost. The electric field distribution of fundamental mode shown in Fig. 1(b) is numerically analyzed by the finite element method (FEM) with the perfect matching layer (PML) as the boundary absorption condition. Simulation results show that the DC-DCPCF maintains single fundamental mode which is well localized in the fiber core region from E to U wavebands. At the same time, the effective refractive index n_{eff} of the fundamental mode can be obtained and fitted using MATLAB. The dispersion D and confinement loss α_c [25] of DC-DCPCF are calculated by:

$$D = -\frac{\lambda}{c}\frac{d^2\mathrm{Re}(n_{eff})}{d\lambda^2}. \quad (2)$$

$$\alpha_c = 8.686 \times 10^6 \frac{2\pi}{\lambda}\mathrm{Im}(n_{eff}). \quad (3)$$

where c is the speed of light, and $\mathrm{Re}(n_{eff})$ and $\mathrm{Im}(n_{eff})$ stand for the real and imaginary part of n_{eff}, respectively. PCF's losses are divided into three main categories: absorption loss, scattering loss and confinement loss. The first two types of losses can be effectively controlled through the design of the fiber structure and strict control of the production process, so confinement loss will be the main consideration.

The dispersion and the dispersion slope change with the wavelength. In order to ensure that dispersion and dispersion slope can be compensated simultaneously in the broadband range, the effective compensated dispersion D_e is usually used to evaluate

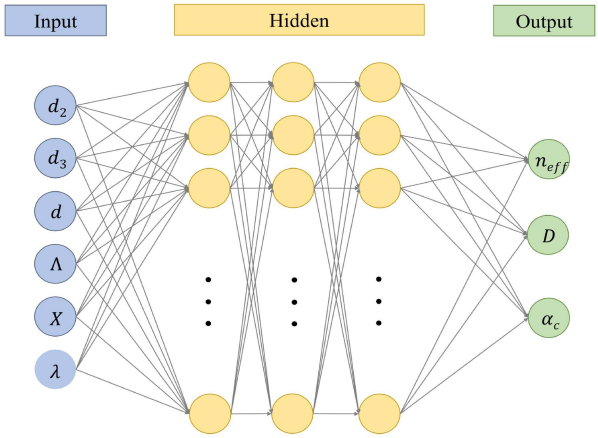

Fig. 2. The topology of DC-DCPCF forward predictive ANN.

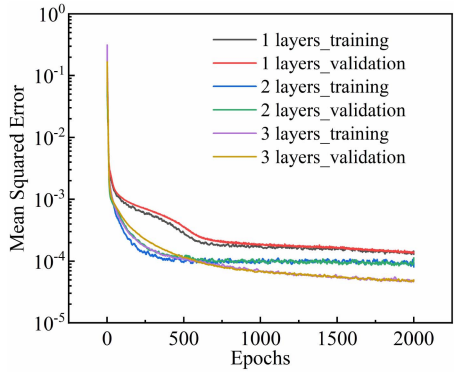

Fig. 3. The MSE for different numbers of hidden layers.

the compensation effect of DC-DCPCF. The smaller D_e indicates the less residual dispersion after dispersion compensation, and the better dispersion compensation performance.

$$D_e = \frac{D_{DC-PCF}L_{DC-PCF} - D_{SMF}L_{SMF}}{L_{DC-PCF} + L_{SMF}}. \quad (4)$$

where D_{DC-PCF} and D_{SMF} stand for the dispersion of DC-DCPCF and SMF28, L_{DC-PCF} and L_{SMF} denote the length of DC-DCPCF and SMF28.

Moreover, the kappa value [26], [27], which indicates the ability to compensate for both dispersion and dispersion slope, should also be approximated with SMF28 at 1.55 μm, and it is given by the formula (5):

$$Kappa = \frac{D_{DC-PCF}}{D_{slope-DC-PCF}}. \quad (5)$$

where $D_{slope-DC-PCF}$ is the dispersion slope of DC-DCPCF. The kappa value of the SMF28 is 297.707nm at 1.55 μm.

The dispersion compensation multiple (DCM) is the ratio of D_{DC-PCF} and D_{SMF}, can be calculated by:

$$DCM = \frac{D_{DC-PCF}}{D_{SMF}}. \quad (6)$$

B. Principle of ANN

In order to solve the problem of time-consuming by using FEM, an ANN model with input layer, output layer and multiple hidden layers is constructed in this paper, and its structure is schematically shown in Fig. 2. The input layer has six neurons corresponding to the design parameters of the DC-DCPCF, which can be represented as [d_2, d_3, d, Λ, X, λ].

The output layer has three neurons corresponding to the properties of the DC-DCPCF, which can be represented as [n_{eff}, D, α_c].

In this paper, the design parameters of DC-DCPCF and the corresponding properties in the range of 1.3 to 1.75 μm were obtained by using COMSOL Multiphysics. A data set which consists of 3050 sets with mapping relationships of design parameters and properties is formed. 80% of the data set are used as the training set, 10% as the validation set and 10% as the test set. The training set is used to update the weights and biases of each hidden layer neuron, the validation set is used to determine whether the ANN is overfitting, and the test set is used to determine the generalization ability of the ANN.

The ReLU function is chosen as the activation function, the Adam algorithm as the optimizer and the mean square error (MSE) function as the loss function. During the training process, MSE between the predicted value and the actual value of DC-DCPCF properties is calculated by using ANN model and backpropagated to update the weights and offsets of neurons of hidden layers. The above process is iterated until convergence.

The number of hidden layers, neurons and training generations in the ANN all have an impact on the convergence of the network and hence on the forward prediction of the ANN. In this paper, we focus on the influence of the number of layers and training generations on the ANN. Fig. 3 shows the convergence of MSE when the number of hidden layers is set to 1, 2 and 3 with 50 neurons of each one.

As seen in Fig. 3, at the beginning of training, the MSE curves of both training and validation data sets for different numbers of hidden layers show a significant decrease. As the number of training generations increases, the decline rate of MSE gradually slows down. When the epoch reaches 500, the MSE gradually converges. When the epoch reaches 2000, the training MSE and validation MSE keep the simultaneous decline with the same decline rate, which indicates that the ANN is not over-fitted and can be considered to converge. At the same time, as the number of hidden layers increases, the MSE can converge to a lower value. The 3-layer hidden layer ANN has the lowest MSE ($< 10^{-4}$) when the epoch reaches 2000.

Therefore, we further evaluated the ANN of the three hidden layers by using the test set. In order to evaluate the forward prediction ability of the ANN more visually, Fig. 4 shows the relationship between the predicted value and the actual value of DC-DCPCF properties.

In Fig. 4, the vertical and horizontal coordinates represent the predicted and actual values of the properties respectively, and each point means a set of predicted-actual values' correspondence. Ideally, the predicted values should fit the actual values to a high degree which stands for each point falling on y = x. Fig. 4 reveals that each data point is almost distributed

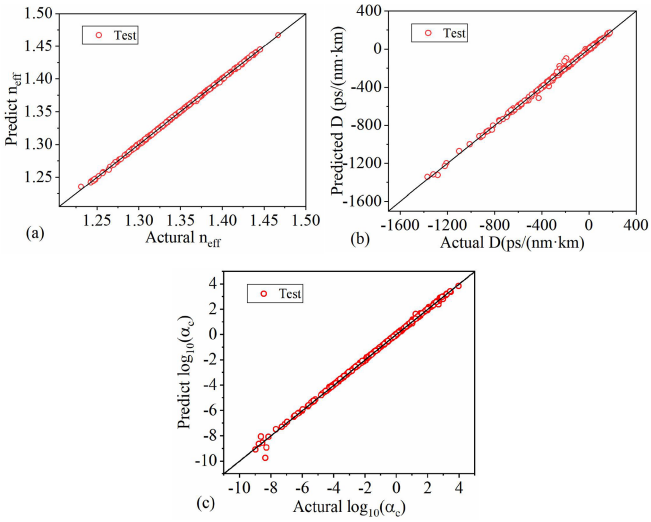

Fig. 4. Relationship between predicted values and actual values of DC-DCPCF properties: (a)n_{eff}. (b)D. (c)α_c.

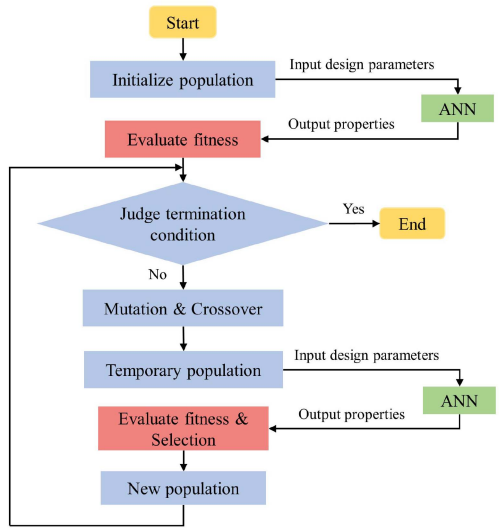

Fig. 5. Flowchart of inverse design of DC-DCPCF based on ANN-DE.

around y = x. The correlation coefficients of n_{eff}, D and α_c between the predicted values and the actual values all exceed 0.999. In Fig. 4(c), although a small number of data deviate from y = x at the left endpoint due to the small number of α_c with minimal values, it does not affect the overall correlation coefficient. It indicates that the ANN with 3 hidden layers establishes a well mapping relationship between the DC-DCPCF design parameters and the properties. It can be used to predict accurately for all 3 properties.

C. Inverse Design Process of DC-DCPCF

The ANN constructed as shown in Fig. 2 is used for the fast prediction of DC-DCPCF properties, and then the proposed DC-DCPCF is inversely designed by using DE. The flowchart is shown in Fig. 5.

TABLE I
DESIGN PARAMETERS' RANGES OF DC-DCPCF

Design parameters	Min	Max
d_2/d	0.50	1.00
d_3/d	0.50	1.00
d_3/d	0.60	0.90
Λ (μm)	0.95	1.20
X	0.10	0.50
λ (μm)	1.36 or 1.46	1.67

1) Initialize population. A population in DE contains NP individuals, each of which is a set of design parameters of DC-DCPCF. NP is set to 50, the scaling factor of DE is set to 0.5, and the hybridization probability CR is set to 0.5. In order to avoid the overlapping of different layers of air holes, the diameters of each layer of air holes are given in DE as relative values, d_2/d, d_3/d and d/Λ, respectively. The design parameters' ranges of DC-DCPCF are shown in Table I.

Therefore, the design parameters of a single initial individual generated by DE can be represented as $[(d_2/d)_0$, $(d_3/d)_0$, $(d/\Lambda)_0$, Λ_0, X_0, $\lambda_0]$. Within the parameter ranges shown in Table I, DE will randomly generate the initial populations.

2) Fast forward predict using ANN. When the properties are forwardly predicted by ANN, the design parameters need to be converted from relative to absolute values and then input to ANN. Due to the matrix operation property of ANN, the properties of DC-DCPCF at the ith wavelength can be solved quickly by using ANN. For a DC-DCPCF population with NP of 50, the corresponding dispersion can be calculated within milliseconds, which accelerates the calculating efficiency of the properties. The properties output from ANN will be entered into the $fitness$ for further calculation and comparison.

3) Evaluate $fitness$. The $fitness$ is defined as the MSE between DC-DCPCF and SMF28:

$$fitness = \frac{1}{N}\sum_{i=1}^{N}\left(W_D(L \times D_i - D_i')^2 + W_{\alpha_c}\alpha_{c_i}\right). \quad (7)$$

where N is the number of wavelength sampling points of the band to be compensated. i ∈ [1, N], represents the ith sampling point. L denotes the distance of SMF28 to be compensated.

D_i and D_i' denote the dispersion of SMF28 and DC-DCPCF at the ith wavelength, respectively, and α_{c_i} denotes the confinement loss of DC-DCPCF. W_D and W_{α_C} are the weight values of the dispersion and confinement loss.

For a SMF28's distance to be compensated L, it is desired to obtain a set of design parameters by using DE, so that the residual dispersion of the DC-DCPCF is near zero. More importantly, the $L \times D_i$ can be extended to any dispersion compensation multiple which means a DC-DCPCF can theoretically be designed to make the residual dispersion near zero with different dispersion characteristics to be compensated.

4) Determine whether the termination condition is satisfied. Set the termination condition of the algorithm to be as small as $fitness$ in the maximum evolutionary generation (500). If the

TABLE II
DC-DCPCF'S DESIGN PARAMETERS FOR DIFFERENT TARGET IN S+C+L+U BANDS

Structure	Target *DCM*	d_2/d	d_3/d	d/Λ	Λ /μm	X /mol%	Total time/s
Structure1	15	0.914	0.971	0.702	1.05	34.7	8.94
Structure2	30	0.730	1.000	0.832	1.03	29.0	8.86
Structure3	45	0.713	0.958	0.884	1.00	20.6	8.96

termination condition is not satisfied, go to step (5), otherwise proceed to step (6).

5) Differential mutation and crossover operations are performed. Then intermediate populations are obtained according to the parameter's optimization range of DC-DCPCF. After fast forward prediction of the temporary population using ANN, the output dispersion will enter the fitness function again for further calculation and comparison (similar to steps (2)–(3)). According to the fitness of DC-DCPCF individuals in the temporary population, the individuals are selected among the initial population and the temporary population to obtain a new generation of population. Finally, return to step (4) to continue to judge whether the termination condition is satisfied.

6) Terminate the evolution and output the parameters of the best individual obtained as the optimal solution which satisfies the broadband DC-DCPCF. Then complete the inverse design.

III. NUMERICAL RESULTS OF DISPERSION COMPENSATION

For S+C+L+U and E+S+C+L+U bands, different targets $DCM$are set respectively, and the target DC-DCPCF is inversely designed by ANN-DE. The broadband dispersion compensation performance of DC-DCPCF, which is inversely designed by ANN-DE, is verified and analyzed by FEM.

A. Dispersion Compensation in S+C+L+U Bands

In S+C+L+U bands, the target DCM is set to 15, 25 and 45 respectively, and the design parameters (d_2/d, d_3/d, d/Λ, Λ, X) obtained by inverse design of the DC-DCPCF are shown in Table II. Additionally, the total time of inverse designing a DC-DCPCF structure by ANN-DE is also shown in Table II.

As can be seen from Table II, the Ge-doped mole fraction of the DC-DCPCF inversely designed by ANN-DE keeps a low level of 20.6∼34.7mol%, which is beneficial to reduce the production cost and fabrication difficulty. Meanwhile, the ANN needs not to be replaced, and it only takes 8∼9 seconds to inversely design a target DC-DCPCF based on ANN-DE, which greatly improves the efficiency of inverse design and has strong reusability.

Using FEM, the broadband dispersion compensation property and confinement loss of three DC-DCPCF structures in S+C+L+U bands inversely designed by ANN-DE is investigated. The results are shown in Fig. 6.

Fig. 6(a) shows the target dispersion and the verified dispersion by FEM, which are represented by points and solid lines respectively, when DCM is set as 15, 30 and 45. It can be seen that the verified dispersion of DC-DCPCF has a good

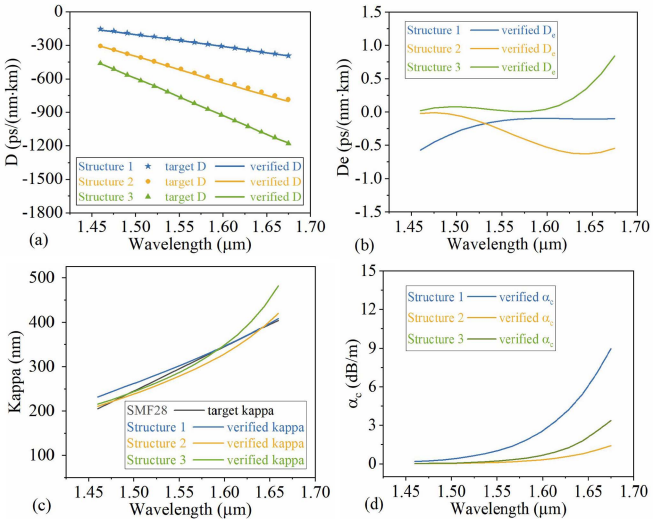

Fig. 6. Results of inversely design DC-DCPCF's dispersion compensation in S+C+L+U bands. (a) Predicted dispersion of DC-DCPCF. (b) D_e. (c) kappa value. (d) α_c.

TABLE III
DC-DCPCF'S DESIGN PARAMETERS FOR DIFFERENT TARGET IN E+S+C+L+U BANDS

Structure	Target *DCM*	d_2/d	d_3/d	d/Λ	Λ /μm	X /mol%	Total time/s
Structure4	10	0.672	0.714	0.735	1.05	34.7	11.97
Structure5	15	0.869	1.000	0.748	1.08	15.9	10.92
Structure6	25	0.750	0.983	0.800	1.03	50.0	10.62

match with the target dispersion. By computation, the average dispersion errors are only 4.74, 1.96 and 0.86%. Fig. 6(b) shows the peak-to-peak values of D_e are only 0.48, 0.69 and 0.84 ps/(nm·km). As DCM increases, the range of D_e increases that the effect of dispersion compensation will gradually become worse within the same bands. But the DC-DCPCF with the highest DCM still maintains a low D_e. It can be seen from Fig. 6(c) that different DC-DCPCFs have good similarity with the kappa values of Corning SMF28.

Therefore, the DC-DCPCF can be inversely designed by ANN-DE with good dispersion compensation when DCM is 15, 30 and 45 respectively. In addition, the confinement loss $\alpha_c$of DC-DCPCF keeps a low level with only 1.05, 0.11 and 0.22 dB/m at 1.55 μm, as can be seen from Fig. 6(d).

B. Dispersion Compensation in E+S+C+L+U Bands

In E+S+C+L+U bands, the target is set to 10, 15 and 25, respectively. The design parameters (d_2/d, d_3/d, d/Λ, Λ, X) obtained by inverse design of the DC-DCPCF and the total time of inversely designing a DC-DCPCF structure by ANN-DE are shown in Table III.

Table III shows that the Ge-doped mole fraction of the DC-DCPCF inversely designed by ANN-DE is only 15.7∼50.0mol%, which contribute to reduce the production cost and fabrication difficulty. The ANN needs not to be replaced,

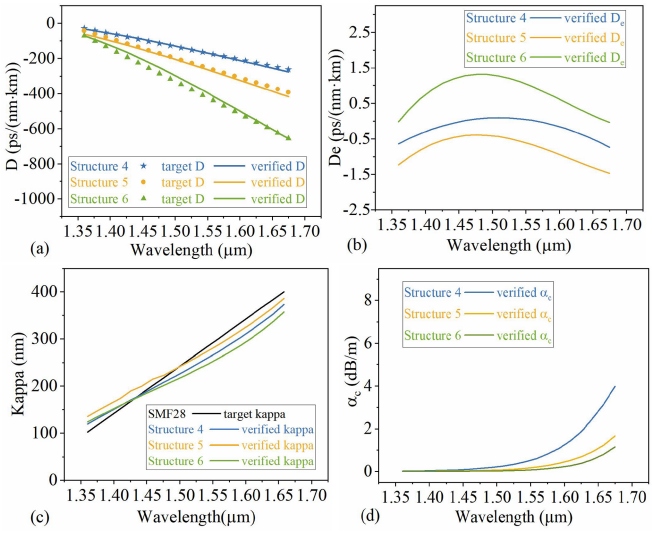

Fig. 7. Results of inversely design DC-DCPCF's dispersion compensation in E+S+C+L+U bands. (a) Predicted dispersion of DC-DCPCF. (b) D_e. (c) kappa value. (d) α_c.

and it takes only 10∼11 seconds which greatly improves the efficiency of inverse design.

The broadband dispersion compensation property and confinement loss of three DC-DCPCF structures in the E+S+C+L+U bands is investigated by FEM. The results are shown in Fig. 7.

Fig. 7(a) shows the target dispersion and the verified dispersion by FEM, which are represented by points and solid lines respectively, when DCM is 10, 15 and 25. It is obvious that the verified dispersion of DC-DCPCF has a good match with the target dispersion. The results indicate that the average dispersion errors of the DC-DCPCF obtained by inverse design are only 2.04, 6.47 and 8.42%. And Fig. 7(b) shows that the peak-to-peak values of D_e are only 0.84, 1.08 and 1.34 ps/(nm·km), respectively. The increase of the DCM and wavebands' range causes a certain deterioration of the dispersion, which induces more difficulties for dispersion compensation compared with the properties in S+C+L+U bands. It can be seen from Fig. 7(c) that, despite the increase of the compensation band, the DC-DCPCF maintains well similarity with the kappa value of SMF28. At 1.55μm, the confinement loss α_c of DC-DCPCF keeps a lower level of 0.52, 0.17 and 0.0747 dB/m compared to S+C+L+U bands as shown in Fig. 7(d).

The compensation performance of the proposed DC-DCPCF is compared with the references in terms of dispersion, DCM, D_e and compensation bands, as shown in Table IV. It can be seen that the DCM of DC-DCPCF inversely designed by ANN-DE in this paper is improved 77.37% over the optimal values of S+C+L+U bands, 47.75% over the optimal value of E+S+C+L+U bands with the PCF designed in the references. Moreover, the effective dispersion D_e of DC-DCPCF in this paper is also reduced 69.67% and 16.25%, respectively. In addition, the kappa values of the DC-DCPCF in this paper and SMF28 are in good match. The results show that the inverse design method of ANN-DE makes a great improvement in design speed and

TABLE IV
COMPARISON OF COMPENSATION PERFORMANCES BETWEEN PROPOSED DC-DCPCF AND OTHER REFERENCES

Reference	D $ps/(nm \cdot km)$	DCM	D_e $ps/(nm \cdot km)$	Compensation bands
[6]	-399.04	15.43	-	S+C
[7]	-440.84	25.37	-0.5 ~ +0.1	S+C+L+U
[8]	-449.38	-	-1.38 ~ +1.38	S+C+L+U
[9]	-294	16.92	-1.5~ +0.1	E+S+C+L+U
Structure 3	-760.05	45	+0.005~ +0.842	S+C+L+U
Structure 6	-366.41	25	-0.03~ +1.31	E+S+C+L+U

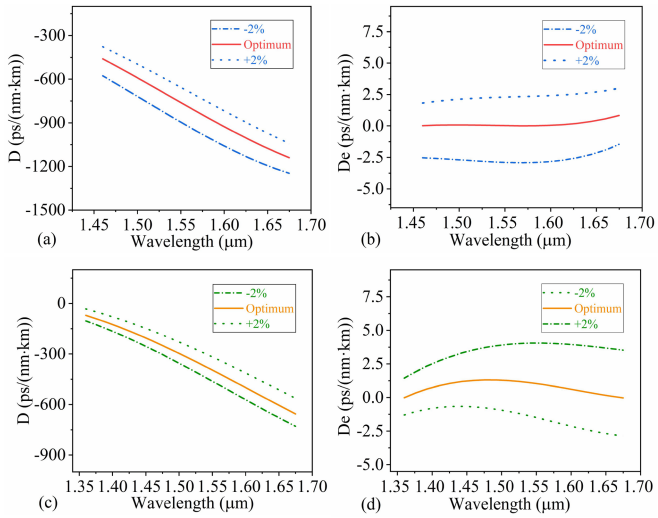

Fig. 8. Influences of the global parameters variation of ±2% on the dispersion curves of DC-DCPCF in different bands. (a) dispersion in S+C+L+U bands. (b) D_e in S+C+L+U bands. (c) dispersion in E+S+C+L+U bands. (d) D_e in E+S+C+L+U bands.

dispersion compensation properties, which cannot be obtained by the traditional control variable method or single optimization algorithm.

C. Fabrication Tolerance

During actual fiber fabrication, there are unavoidable structural variations that have certain effects on the fiber dispersion characteristics. It is known that the fabrication tolerance of the structural parameters can be controlled to within ±1% through existing fabrication technique which have a large design flexibility [28], [29]. But the influences of the fabrication tolerance of the DC-DCPCF on the dispersion characteristics cannot be neglected. For this reason, the dispersion and D_e curves obtained by fabrication tolerance of ±2% global parameters' variation for the optimum in S+C+L+U and E+S+C+L+U bands are demonstrated in Fig. 8.

Fig. 8(a) and (c) show that the dispersion curve will shift up and down as a whole when all of the geometric parameters change ±2%. The dispersion varies from −376.98 to −1041.41ps/(nm·km) and −557.33 to −1234.90ps/(nm·km) in S+C+L+U bands. And the dispersion varies from −32.83 to

−563.33ps/(nm·km) and −104.25 to −729.35ps/(nm·km) in E+S+C+L+U bands. The results show that the dispersion of the designed DC-DCPCF remains linear for ±2% variation of the structural parameters. Besides, D_e curves also show within −2.92 to +2.99ps/(nm·km) and −2.85 to +3.98 ps/(nm·km) over the S+C+L+U and E+S+C+L+U bands in Fig. 8(b) and (d), respectively. It is worth noting that the variation of the global geometry parameters helps to provide an upper limit to the severity of manufacturing defects. Because in reality not all parameters are distorted from their optimal values in the same way and some averaging effects may occur. Therefore, the proposed DC-DCPCF can still be competent for dispersion compensation under fabrication tolerance.

IV. Conclusion

In this paper, the broadband DC-DCPCF with five layers of triangular air holes and low Ge-doped cladding has been proposed. The design parameters of the DC-DCPCF are inversely designed based on ANN-DE, and the dispersion compensation property in S+C+L+U and E+S+C+L+U bands is analyzed. The results show that the DC-DCPCF inversely designed by ANN-DE is highly similar to the target in just ten seconds and demonstrates good broadband dispersion compensation. It has a low effective compensated dispersion with only +0.005∼+0.842 ps/(nm·km) in S+C+L+U bands and low confinement loss with 0.22 dB/m at 1.55μm when the dispersion compensation multiple reaches up to 45. In E+S+C+L+U bands, it can compensate 25 times the length of SMF28 with −0.03∼+1.31 ps/(nm·km) of effective compensated dispersion and 0.0747dB/m of confinement loss at 1.55μm. The Ge-doped mole fraction of DC-DCPCF is maintained at 15.7 mol% to 50 mol% for both bands. In addition, the kappa values are also highly good match with those of SMF28 that satisfy broadband dispersion and dispersion slope compensation simultaneously. An automated DC-DCPCF design method is constructed for SMF28 to enable arbitrary wavebands and dispersion compensation multiples and has a wide application prospect in the fields of Raman amplifiers, fiber gratings, optical sensors and other photonic integrated systems.

References

[1] K. Saitoh, M. Koshiba, T. Hasegawa, and E. Sasaoka, "Chromatic dispersion control in photonic crystal fibers: Application to ultra-flattened dispersion," *Opt. Exp.*, vol. 11, no. 8, pp. 843–852, Apr. 2003.

[2] F. Begum, Y. B. Zsigri, J. Lgsgaard, and A. Bjarklev, "A novel photonic crystal fibre design for dispersion compensation," *J. Opt. A: Pure Appl. Opt.*, vol. 6, no. 7, pp. 717–720, Jul. 2004.

[3] F. Begum et al., "Novel broadband dispersion compensating photonic crystal fibers: Applications in high-speed transmission systems," *Opt. Laser Technol.*, vol. 41, no. 6, pp. 679–686, Sep. 2009.

[4] X. Zhao et al., "Photonic crystal fiber for dispersion compensation," *Appl. Opt.*, vol. 47, no. 28, pp. 5190–5196, Sep. 2008.

[5] L. P. Shen, W. P. Huang, and G. X. Chen, "Design and optimization of photonic crystal fibers for broad-band dispersion compensation," *IEEE Photon. Technol. Lett.*, vol. 15, no. 4, pp. 540–542, Apr. 2003.

[6] W. Wang et al., "Novel design of broadband dispersion compensating photonic crystal fiber with all solid structure and low index difference," *Optik*, vol. 156, pp. 279–288, Mar. 2018.

[7] W. Y. Sun, Y. H. Qu, J. S. Cao, and H. Z. Jia, "Sandwiched photonic crystal fiber for dispersion compensation over the S+C+L+U wavelength bands," *Appl. Opt.*, vol. 60, no. 18, pp. 5399–5404, Jun. 2021.

[8] H. Z. Xu, Q. L. Kong, and C. J. Zhou, "Crossings in photonic crystal fiber with hybrid core and design of broadband dispersion compensating photonic crystal fiber," *Opt. Fiber Technol.*, vol. 63, 2021, Art. no. 102485.

[9] M. S. Habib, M. S. Rana, M. Moniruzzaman, M. S. Ali, and N. Ahmed, "Highly birefringent broadband dispersion compensating photonic crystal fiber over the E+S+C+L+U wavelength bands," *Opt. Fiber Technol.*, vol. 20, no. 5, pp. 527–532, Oct. 2014.

[10] L. Cherbi, A. Bellalia, L. Bahloul, M. Touzene, and M. Lamara, "Characterization of the propagation in photonic crystal fibers with the scalar-finite element method," *SPIE*, vol. 8426, pp. 209–220, 2012.

[11] C. C. Nadell, B. H. Huang, J. M. Malof, and W. J. Padilla, "Deep learning for accelerated all-dielectric metasurface design," *Opt. Exp.*, vol. 27, no. 20, pp. 27523–27535, Sep. 2019.

[12] K. Yao, K, R. Unni, and Y. B. Zheng, "Intelligent nanophotonics: Merging photonics and artificial intelligence at the nanoscale," *Nanophotonics*, vol. 8, no. 3, pp. 339–366, Mar. 2019.

[13] B. Karanov et al., "End-to-end deep learning of optical fiber communications," *J. Lightw. Technol.*, vol. 36, no. 20, pp. 4843–4855, Oct. 2018.

[14] D. Rafique, T. Szyrkowiec, H. Grieber, A. Autenrieth, and J. P. Elbers, "Cognitive assurance architecture for optical network fault management," *J. Lightw. Technol.*, vol. 36, no. 7, pp. 1443–1450, Apr. 2018.

[15] Z. Q. He et al., "Machine learning aided inverse design for few-mode fiber weak-coupling optimization," *Opt. Exp.*, vol. 28, no. 15, pp. 21668–21681, Jul. 2020.

[16] Z. N. Wang, J. B. Du, W. H. Shen, J. C. Liu, and Z. Y. He, "Efficient design for integrated photonic waveguides with agile dispersion," *Sensors*, vol. 21, no. 19, Oct. 2021.

[17] Y. Long, J. Ren, Y. H. Li, and H. Chen, "Inverse design of photonic topological state via machine learning," *Appl. Phys. Lett.*, vol. 114, no. 18, May 2019, Art. no. 181105.

[18] D. Zibar, A. M. R. Rosa Brusin, U. C. de Moura, F. Da Ros, V. Curri, and A. Carena, "Inverse system design using machine learning: The Raman amplifier case," *J. Lightw. Technol.*, vol. 38, no. 4, pp. 736–753, Feb. 2020.

[19] M. A. Jabin and M. P. Fok, "Prediction of 12 photonic crystal fiber optical properties using MLP in deep learning," *IEEE Photon. Technol. Lett.*, vol. 34, no. 7, pp. 391–394, Apr. 2022.

[20] S. Chugh, A. Gulistan, S. Ghosh, and B. M. A. Rahman, "Machine learning approach for computing optical properties of a photonic crystal fiber," *Opt. Exp.*, vol. 27, no. 25, pp. 36414–36425, Jan. 2019.

[21] Z. H. Ma and Y. Li, "Parameter extraction and inverse design of semiconductor lasers based on the deep learning and particle swarm optimization method," *Opt. Exp.*, vol. 28, no. 15, pp. 21971–21981, Jul. 2020.

[22] H. W. Icenogle, B. C. Platt, and W. L. Wolfe, "Refractive indexes and temperature coefficients of germanium and silicon," *Appl. Opt.*, vol. 15, no. 10, pp. 2348–2351, Oct. 1976.

[23] S. Ju et al., "Effect of Ge nanoparticles in the core of photonic crystal fiber on supercontinuum generation," *J. Nanomater.*, vol. 2019, 2019, Art. no. 6824059.

[24] H. Z. Xu, X. L. Wang, X. L. Huang, C. J. Zhou, H. L. Zhu, and X. M. Cai, "All-solid photonic crystal fiber for dispersion compensation over S+C+L wavelength bands," *IEEE Photon. Technol. Lett.*, vol. 30, no. 17, pp. 1499–1502, Sep. 2018.

[25] F. Begum, Y. Namihira, S. M. A. Razzak, and N. Y. Zou, "Novel square photonic crystal fibers with ultra-flattened chromatic dispersion and low confinement losses," *IEICE Trans. Electron.*, vol. 90, no. 3, pp. 607–612, Mar. 2007.

[26] S. G. Li, X. D. Liu, and L. T. Hou, "Numerical study on dispersion compensating property in photonic crystal fibers," *Acta Physica Sinica*, vol. 53, no. 6, pp. 1880–1886, Feb. 2004.

[27] C. Wang, Y. J. Zhang, Z. Wu, G. Zhang, Y. Zhang, and L. Jiang, "Design of all-solid dual-concentric-core microstructure fiber for ultra-broadband dispersion compensation," *Appl. Sci.*, vol. 9, no. 16, pp. 3366–3375, Aug. 2019.

[28] F. Poletti, V. Finazzi, T. M. Monro, and N. G. R. Broderick, "Inverse design and fabrication tolerances of ultra-flattened dispersion holey fibers," *Opt. Exp.*, vol. 13, no. 10, pp. 3728–3736, Apr. 2005.

[29] W. H. Reeves, J. C. Knght, and P. S. J. Russell, "Demonstration of ultra-flattened dispersion in photonic crystal fibers," *Opt. Exp.*, vol. 10, no. 14, pp. 609–613, Jul. 2002.